IOPscience iopscience.iop.org

Home Search Collections Journals About Contact us My IOPscience

X-ray scattering study of interface structures in Si-$Si_{1-x}Ge_x$ superlattices grown on vicinal Si(111) substrates

This article has been downloaded from IOPscience. Please scroll down to see the full text article.

2001 J. Phys.: Condens. Matter 13 8733

(http://iopscience.iop.org/0953-8984/13/39/302)

View the table of contents for this issue, or go to the journal homepage for more

Download details:
IP Address: 171.66.16.226
The article was downloaded on 16/05/2010 at 14:54

Please note that terms and conditions apply.

INSTITUTE OF PHYSICS PUBLISHING JOURNAL OF PHYSICS: CONDENSED MATTER

J. Phys.: Condens. Matter **13** (2001) 8733–8744 PII: S0953-8984(01)23554-1

X-ray scattering study of interface structures in Si–$Si_{1-x}Ge_x$ superlattices grown on vicinal Si(111) substrates

Y Yamaguchi[1] **and H Hashizume**[2]

Materials and Structure Laboratory, Tokyo Institute of Technology, Nagatsuta, Midori, Yokohama 226-8503, Japan

E-mail: hhashizu@ms.aist-nara.ac.jp

Received 29 March 2001, in final form 17 July 2001
Published 13 September 2001
Online at stacks.iop.org/JPhysCM/13/8733

Abstract

The interface structures of Si–$Si_{1-x}Ge_x$ ($x = 0.1, 0.3$) superlattices grown on vicinal Si(111) substrates are determined from grazing-angle x-ray scattering data. Diffuse intensity distributions in reciprocal space are calculated using new formulae developed to explicitly take account of the partially correlated periodic roughness due to the substrate miscut and the step bunching, in addition to random roughness. The calculated intensity maps well explain the experimental ones observed from the Si–$Si_{0.9}Ge_{0.1}$ and Si–$Si_{0.7}Ge_{0.3}$. The bunched steps at the substrate Si(111) surface are widely dispersed at the Si/$Si_{0.7}Ge_{0.3}$ interfaces, while the bunched step structure is replicated onto the Si/$Si_{0.9}Ge_{0.1}$ interfaces. The different step configurations are ascribed to the three-times greater misfit strain in the Si–$Si_{0.7}Ge_{0.3}$. The two interfaces have distinct in-plane terrace/stepped area ratios of ∼3 and 0.35–0.7. The periodic terrace–step structures are equally well correlated in the two supelattices in the out-of-plane direction, while the random roughness has smaller correlation lengths in the Si–$Si_{0.9}Ge_{0.1}$ than in the Si–$Si_{0.7}Ge_{0.3}$.

1. Introduction

Controlling interface structures is a key technique in applications of Si–$Si_{1-x}Ge_x$ heterostructures to optoelectronics and high-speed electronics. Interface roughness scatters charge carriers and thus plays an important role in the device properties. The lattice-constant mismatch between Si and $Si_{1-x}Ge_x$ strains thin layers and this strain affects the surface and interface morphology of the Si–$Si_{1-x}Ge_x$ superlattice depending upon x [1, 2]. The tensile

[1] Present address: Elm Technology, 6-67 Kagurazaka, Shinjuku, Tokyo 162-0825, Japan.
[2] Present address: Research and Education Center for Materials Science, Nara Institute of Science and Technology, Takayama, Ikoma 630-0101, Japan.

0953-8984/01/398733+12$30.00 © 2001 IOP Publishing Ltd Printed in the UK

and compressive stress fields, induced in the Si and $Si_{1-x}Ge_x$ layers respectively, influence the configuration of atomic steps at the Si/SiGe interface. It is well known that a $Si_{1-x}Ge_x$ layer grown on a Si layer shows a rougher surface than a Si layer on a $Si_{1-x}Ge_x$. Our previous work [3, 4] demonstrates that a Si–$Si_{0.9}Ge_{0.1}$ superlattice and a Si–$Si_{0.7}Ge_{0.3}$ superlattice, grown on similar vicinal Si(111) substrates, have markedly different terrace–step structures at the layer interfaces. The three-times greater misfit strain would have promoted a redistribution of the steps replicated from the substrate surface in the Si–$Si_{0.7}Ge_{0.3}$. The Si/SiGe interfaces in these samples include random roughness, in addition to the periodic terrace–step structures due to the finite miscut angle of the substrate surface, as evidenced by the x-ray data. Each component has partially correlated structures along the in-plane and out-of-plane directions. X-ray scattering is a powerful technique to explore buried interface structures with high momentum and real-space resolutions, but it is a challenge to quantitatively characterize this type of structure. Holý *et al* [5] put forward a theory of x-ray scattering for multilayers with stepped interfaces. In this paper, we present in section 3 a new formulation that explicitly takes into account the random and periodic components of interface roughness and thus is more appropriate than Holý *et al*'s formulation to our Si–$Si_{1-x}Ge_x$ samples. We apply our theory in section 4 to high-resolution x-ray diffuse scattering data collected at a synchrotron source. This paper starts by describing the x-ray experiment in section 2.

2. Experiment and results

The $[Si–Si_{0.9}Ge_{0.1}]_{10}$ and $[Si–Si_{0.7}Ge_{0.3}]_{10}$ superlattice samples investigated have previously been described [3, 4]. Briefly, they have Si and $Si_{1-x}Ge_x$ layers of a nearly equal nominal thickness of 5 nm, grown by solid-source molecular-beam epitaxy (MBE) on vicinal Si(111) substrates at 500 °C. The growth rate is 0.1 nm s^{-1} for the Si and $Si_{1-x}Ge_x$ layers. The first grown layer is $Si_{1-x}Ge_x$ and a Si layer terminates the superlattice. The substrate surface in each sample is misoriented by 0.6° from the (111) plane in a direction 10° off the $[\bar{2}11]$. The superlattices with Ge contents $x = 0.1$ and $x = 0.3$ are called sample 1 and sample 2 respectively, as in [4]. We carried out x-ray experiments on two bending-magnet beamlines at the 2.5 GeV synchrotron source of the Photon Factory, KEK, Tsukuba, Japan: beamline 4C for sample 1 and beamline 20B for sample 2. Each line is equipped with a focusing mirror and a Si(111) double-crystal monochromator. The x-ray wavelengths used differ slightly: $\lambda = 0.13$ nm on BL-4C and $\lambda = 0.17$ nm on BL-20B. On BL-4C, a slit-limited 1 (horizontal) × 0.17 (vertical) mm^2 beam illuminated a sample on a Huber four-circle goniometer. On BL-20B, the probing beam was 4 (horizontal) × 0.1 (vertical) mm^2 in size and a sample was mounted on the two-axis diffractometer BIGDIFF [6]. Slits were used for the analyser to achieve a geometrical resolution of $\Delta Q_{\parallel} = 3.0 \times 10^{-5}$–$7.5 \times 10^{-4}$ nm^{-1} in the dispersion plane and $\Delta Q_{\perp} = 8.4 \times 10^{-3}$ nm^{-1} in the perpendicular direction on BL-4C. The resolution was $\Delta Q_{\parallel} = 1.6 \times 10^{-5}$–$3.9 \times 10^{-4}$ nm^{-1} and $\Delta Q_{\perp} = 4.4 \times 10^{-3}$ nm^{-1} on BL-20B. The different experimental conditions on the two beamlines are unimportant in the discussion that follows. Three types of scan were carried out: (1) specular scans with $\theta_1 = \theta_2$, (2) offset specular scans with a constant off-specular angle $\Delta\theta = 0.05°$ on a sample ($\theta_1 \neq \theta_2$), and (3) sample rocking scans with fixed detector angles 2θ. Here θ_1 and θ_2 are the angles that the incoming and outgoing x-ray beams make to the sample surface, respectively ($\theta_1 + \theta_2 = 2\theta$). We define the x, y, z coordinates fixed to the sample surface (figure 1), and denote q_x, q_y, q_z the x, y, z components of the scattering vector $\boldsymbol{q}$, respectively. The x axis is parallel to the mean surface and is directed along the substrate miscut direction. The specular scan explores reciprocal space along the q_z axis parallel to the surface normal at $q_x = 0$ or $q_y = 0$, while the offset specular scan traces a radial line inclined from the q_z axis by $\Delta\theta$. Tracks of the

rocking scans are nearly parallel to the q_x or q_y axes. We collected x-ray data in two azimuthal orientations of a sample. In configuration A, the dispersion plane is parallel to the substrate miscut direction, whereas it is perpendicular to the miscut direction in configuration B. This allows us to map the diffuse intensity in the (q_x, q_z) plane and the (q_y, q_z) plane in reciprocal space. Rocking scans in configurations A and B are called q_x scans and q_y scans, respectively.

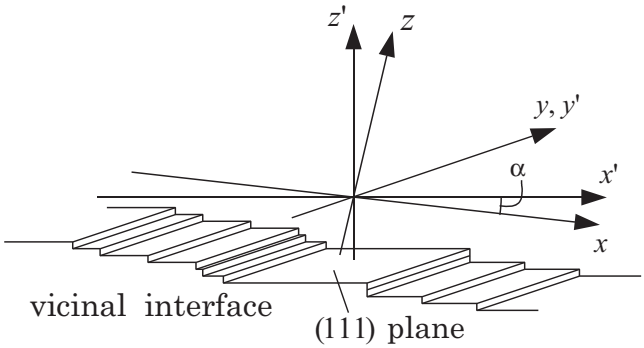

Figure 1. Definition of the coordinate systems. The x, y, z axes are defined by the mean sample surface, while the x', y', z' axes are parallel to the crystallographic directions. α is the angle between the terrace levels and the mean surface.

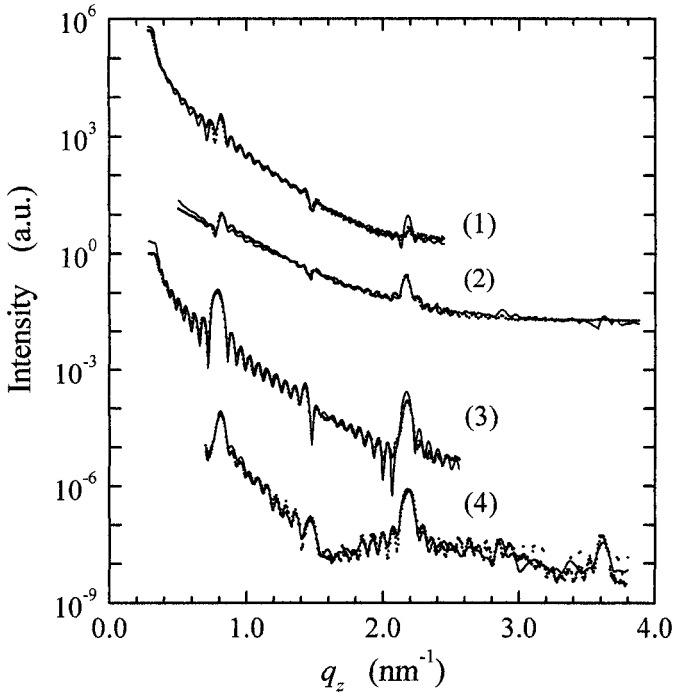

Figure 2. Observed (dots) and calculated (curves) specular (1), (2) and off-specular (3), (4) reflectivity profiles. Curves (1) and (3) are for sample 1, curves (2) and (4) for sample 2. The off-specular scans are offset along the q_x direction. The curves are arbitrarily shifted in the vertical direction for clarity.

Figure 2 shows the results of the specular scans and the offset specular scans for the two samples. The offset angle $\Delta\theta = 0.05^\circ$ used is large enough to exclude the specular intensity. Even-order superlattice Bragg peaks are small because of the nearly equal thicknesses of the pure Si layers and the alloy $Si_{1-x}Ge_x$ layers. The global decay rate of specular intensity is similar in samples 1 and 2, suggesting similar interface roughness in the two samples. The strong Bragg-like peaks seen in the offset specular profiles indicate the significant correlation of the interface roughness in the out-of-plane direction [7]. Figure 3 shows the typical q_x-scan and q_y-scan profiles observed around the third-order superlattice Bragg peaks ($q_z = 2.2\ \mathrm{nm}^{-1}$) for sample 1 (figure 3(a)) and sample 2 (figure 3(b)). Beside the specular peaks at $q_x = 0$ or $q_y = 0$ and the Yoneda peaks at the extremities of each scan, pronounced diffuse peaks (indicated by thick arrows) are observed on several scans. The separations of these peaks in the q_x profiles give the in-plane repeat periods of regular structures at the $Si/Si_{1-x}Ge_x$ interfaces: $\overline{L}_x = 380$ nm for sample 1 and $\overline{L}_x = 1.1\ \mu$m for sample 2. As the atomic-force-microscopy (AFM) trace in figure 4 indicates, the interface morphology consists of long periodic structures and short random corrugations. The periodic component arises from bunched step structures [4] and $\overline{L}_x$ corresponds to the mean period of these structures. The formula $n = \overline{L}_x\alpha/h_s$ gives $n = 13$ for sample 1 and $n = 39$ for sample 2, where α is the miscut angle, h_s is the elementary step height, and n is the mean step number contained in $\overline{L}_x$. In the q_x profiles for sample 1 (figure 3(a)), diffuse peaks are symmetrically located with respect to $q_x = 0$, with distinct heights in the $+q_x$ and $-q_x$ regions. A similar but much less pronounced feature is observed in sample 2 (figure 3(b)). On the q_y scans, on the other hand, no marked diffuse peak is seen in sample 2, but small diffuse peaks are observed in sample 1. The latter is supposed to arise from meandering step lines along the y direction.

The asymmetric diffuse intensity distribution is more clearly seen in the grey-scale maps of figure 5, which covers smaller (q_x, q_z) and (q_y, q_z) areas around the third-order Bragg peaks than figure 3; figures 5(a) and 5(b) are for sample 1 and sample 2, respectively. The skew 'smile' contours of diffuse intensity seen in figure 5(a) indicate that the roughness structures of the different $Si/Si_{0.9}Ge_{0.1}$ interfaces in sample 1 are correlated along a direction off the surface normal (figure 6).

3. Theory of x-ray diffuse scattering

We assume that the regularly stacked Si and $Si_{1-x}Ge_x$ layers are uniform in electron density with abrupt, rough interfaces between them. In this case, x-ray diffuse scattering from a superlattice is dictated by the Fourier transform $\tilde{C}(q_x, q_y, q_z)$ of the height–height correlation function $C(x, y, z)$ describing the interface morphology. $\tilde{C}(q_x, q_y, q_z)$ is called power spectral density function. Since the instrument angular resolution integrates the scattering intensity in the direction perpendicular to the dispersion plane, we are only interested in $\tilde{C}(q_x, q_z)$ and $\tilde{C}(q_y, q_z)$. We discuss $\tilde{C}(q_x, q_z)$ first. For the local height $z_j(x)$ of interface j at point x, we write

$$z_j(x) = z_j^{\mathrm{p}}(x) + z_j^{\mathrm{r}}(x) \tag{1}$$

where $z_j^{\mathrm{p}}(x)$ and $z_j^{\mathrm{r}}(x)$ are the periodic and random components, respectively (figure 4). Correspondingly, the in-plane correlation function for interface j is given by

$$C_{jj}(x, z) = C_{jj}^{\mathrm{p}}(x, z) + C_{jj}^{\mathrm{r}}(x) \tag{2}$$

where $C_{jj}^{\mathrm{p}}(x, z)$ and $C_{jj}^{\mathrm{r}}(x)$ are the in-plane correlation functions for the periodic and random roughnesses, respectively. There would be no correlation between the two types of roughness.

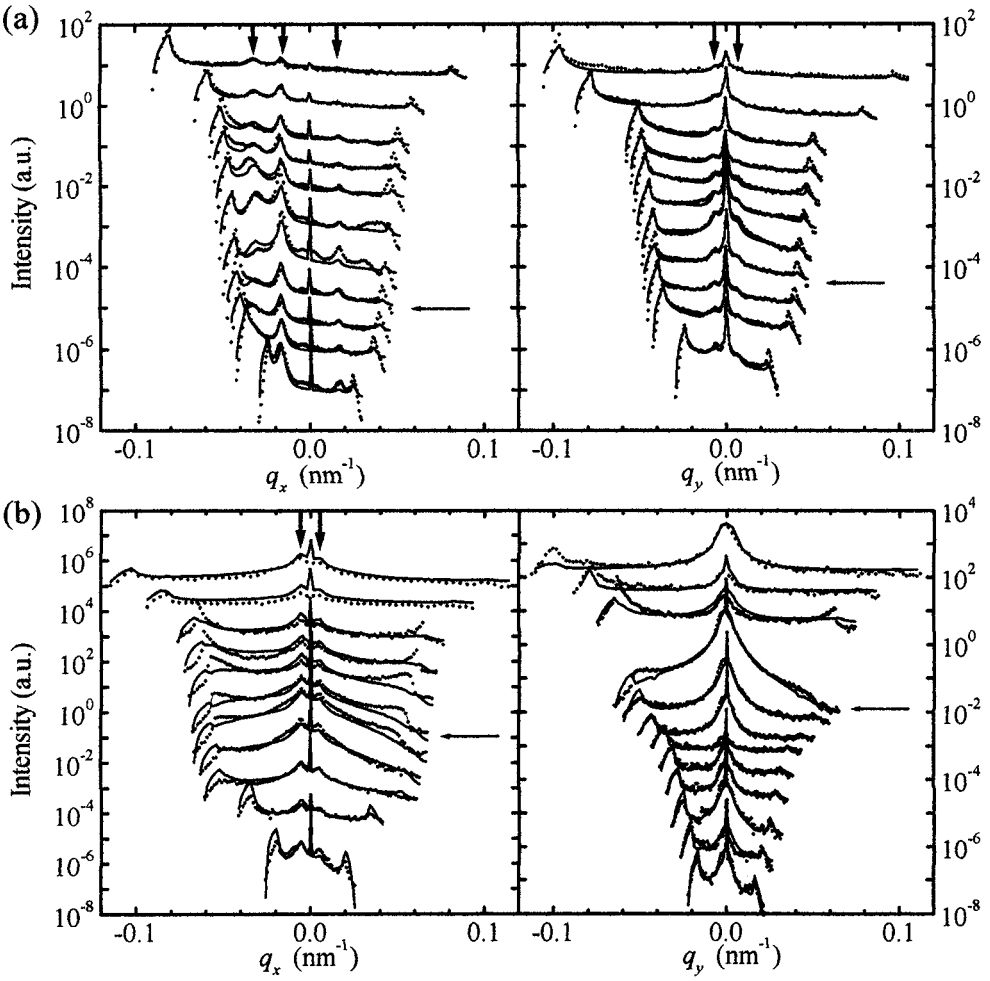

Figure 3. Observed (dots) and calculated (curves) transverse-scan profiles around the third-order superlattice Bragg peaks, (a) for sample 1 and (b) for sample 2. The scattering plane is parallel (left-hand panels) and perpendicular (right-hand panels) to the miscut direction of the substrate surface. The subsidiary peaks are marked by thick arrows on both sides of the specular peaks at $q_x = 0$ or $q_y = 0$. Scans cutting through the third-order Bragg peaks are indicated by fine, horizontal arrows. The q_z coverage is 1.69–2.95 nm^{-1} in the upper-left panel, 1.69–3.21 nm^{-1} in the upper-right panel, 1.36–2.88 nm^{-1} in the bottom-left panel, and 1.26–2.85 nm^{-1} in the bottom right panel. Curves are arbitrarily shifted in the vertical direction in each panel.

$C^{\mathrm{r}}_{jj}(x)$ is defined by

$$C^{\mathrm{r}}_{jj}(x) = \langle z^{\mathrm{r}}_j(x') z^{\mathrm{r}}_j(x'+x)\rangle \tag{3}$$

which is the two-point height-height correlation for separation x. The self-affine fractal model of random roughness gives [8]

$$C^{\mathrm{r}}_{jj}(X) = (\sigma^{\mathrm{r}}_j)^2 \exp[-(x/\xi^{\mathrm{r}}_x)^{2h_{\mathrm{H}}}] \tag{4}$$

where $(\sigma^{\mathrm{r}}_j)^2$ is the mean-square roughness $\langle |z^{\mathrm{r}}_j(x)|^2\rangle$, ξ^{r}_x is the in-plane cutoff length of random roughness along the x direction and h_{H} is the Hurst parameter. For the periodic roughness, we

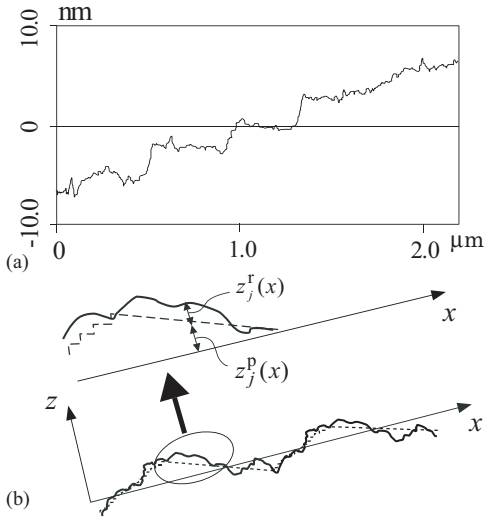

Figure 4. AFM trace along the miscut direction of sample 1 (a) and the scheme defining periodic $z_j^p(x)$ and random $z_j^r(x)$ roughness component (b).

assume

$$C_{jj}^{\mathrm{p}}(x,z) = (\sigma_j^{\mathrm{p}})^2 S_{jj}(x,z) \tag{5}$$

where $(\sigma_j^{\mathrm{p}})^2 = \langle |z_j^{\mathrm{p}}(x)|^2 \rangle$ and $S_{jj}(x,z)$ is the probability with which we find a pair of points separated by (x,z) on interface j. Vicinal Si(111) surfaces often show bunched-step structures, with heavily stepped areas separated by relatively flat terraces parallel to the (111) plane [4, 9, 10]. For ideal vicinal interfaces with an identical step-terrace structure repeating with period $\overline{L}_x$, we may write

$$C_{jj}^{\mathrm{p}}(x,z) = (\sigma_j^{\mathrm{p}})^2 S_{jj}(x,z) \otimes \delta(x - n\overline{L}_x) \tag{6}$$

where $\otimes$ stands for convolution and $\delta(x)$ is a δ function. Pukite *et al* [11] gave

$$\tilde{S}_{jj}(q_{x'}, q_{z'}) = \frac{2}{q_{x'}^2 \bar{l}} \mathrm{Re}\left[\frac{(1-\tilde{P}(q_{x'}))(1-\tilde{H}(q_{z'}))}{1-\tilde{P}(q_{x'})\tilde{H}(q_{z'})}\right] \tag{7}$$

where $\bar{l}$ is the mean terrace width and $\tilde{P}(q_{x'})$ and $\tilde{H}(q_{z'})$ are the Fourier transforms of $P(l)$ and $H(h)$, respectively. Here $P(l)$ is the function describing the statistical distribution of terrace width l, whereas $H(h)$ represents the distribution of step height h. The (x', z') coordinate is defined in figure 1, where the x' and z' axes are parallel and normal to the terraces, respectively. The x' axis is along the miscut direction, making angle α to the x axis. $q_{x'}$ and $q_{z'}$ are related to q_x and q_z by

$$\begin{pmatrix} q_{x'} \\ q_{z'} \end{pmatrix} = \begin{pmatrix} \cos\alpha & \sin\alpha \\ -\sin\alpha & \cos\alpha \end{pmatrix} \begin{pmatrix} q_x \\ q_z \end{pmatrix}. \tag{8}$$

Using equation (7) with equation (6), we find the Fourier transform of $C_{jj}^{\mathrm{p}}(x,z)$ given by

$$\tilde{C}_{jj}^{\mathrm{p}}(q_x, q_z) = \frac{2(\sigma_j^{\mathrm{p}})^2}{q_{x'}^2 \bar{l}} \mathrm{Re}\left[\frac{(1-\tilde{P}(q_{x'}))(1-\tilde{H}(q_{z'}))}{1-\tilde{P}(q_{x'})\tilde{H}(q_{z'})}\right] \mathrm{e}^{-\mathrm{i}q_x \overline{L}_x} \mathrm{e}^{-q_x^2 \tau_x^2} \tag{9}$$

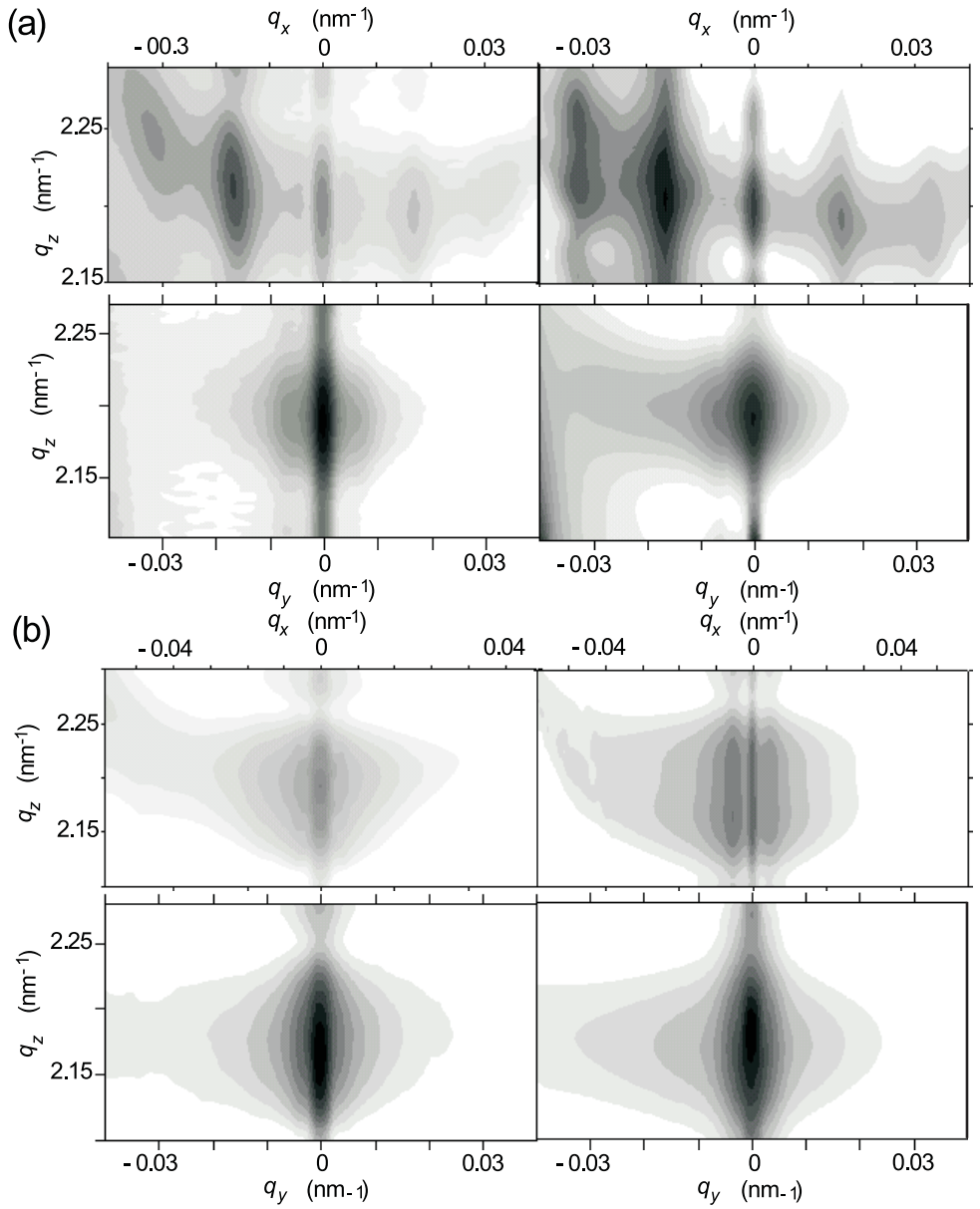

Figure 5. Observed (left-hand panels) and calculated (right-hand panels) diffuse intensity contours around the third-order Bragg peaks in reciprocal space, (a) for sample 1 and (b) for sample 2. In each of (a) and (b) the upper panels show the (q_x, q_z) maps while the lower panels show the (q_y, q_z) maps.

where we have appended $e^{-q_x^2\tau_x^2}$ to account for the fluctuation of L_x around $\overline{L}_x$. $\tilde{C}^{\mathrm{p}}_{jj}(q_x, q_z)$ produces sharp peaks at $q_x = 2\pi/\overline{L}_x$ because of the term $e^{-iq_x\overline{L}_x}$. The in-plane power spectral density function is given by

$$\tilde{C}_{jj}(q_x, q_z) = \tilde{C}^{\mathrm{p}}_{jj}(q_x, q_x) + \tilde{C}^{\mathrm{r}}_{jj}(q_x) \tag{10}$$

where $\tilde{C}^{\mathrm{r}}_{jj}(q_x)$ is the Fourier transform of equation (4).

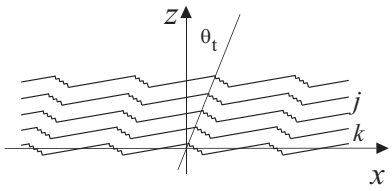

Figure 6. The out-of-plane correlation inclined by angle θ_t off the mean-surface normal.

We now discuss the out-of-plane roughness correlation. Suppose point A_j and point B_k, separated by vector $\boldsymbol{r}(x, Z)$, are located on interfaces j and k at mean heights $\overline{Z}_j$ and $\overline{Z}_k$ respectively (figure 7). To work out a practical form of the two-point correlation function $C_{jk}(x, Z)$, we shift interface j to the location of interface k so that the mean plane of the shifted interface coincides with the one of interface k. The shift direction, indicated by vector $\boldsymbol{r}'(= \boldsymbol{r}'(x', Z'))$ in figure 7, makes an angle θ_t to the Z axis. This translation moves point A_j to point A'_j in figure 7. $C_{jk}(x, Z)$ is given by

$$C_{jk}(x, Z) = I_{jk}(x - x', Z - Z')\delta(x' - |\overline{Z}_j - \overline{Z}_k| \tan\theta_t)\delta(Z' - |\overline{Z}_j - \overline{Z}_k|) \tag{11}$$

where $I_{jk}(x - x', Z - Z')$ is the 'in-plane' height–height correlation between shifted interface j and interface k or between points A'_j and B_k separated by $(x - x', Z - Z')$. After Schromka *et al* [12], we write $I_{jk}(x, z)$ as

$$\begin{aligned} I_{jk}(x, z) = {} & \frac{1}{2}\left[\frac{\sigma_k^{\mathrm{p}}}{\sigma_j^{\mathrm{p}}} C_{jj}^{\mathrm{p}}(x, z) + \frac{\sigma_j^{\mathrm{p}}}{\sigma_k^{\mathrm{p}}} C_{kk}^{\mathrm{p}}(x, z)\right] \mathrm{e}^{-|\overline{Z}_j - \overline{Z}_k|/\xi_z^{\mathrm{p}}} \\ & + \frac{1}{2}\left[\frac{\sigma_k^{\mathrm{r}}}{\sigma_j^{\mathrm{r}}} C_{jj}^{\mathrm{r}}(x) + \frac{\sigma_j^{\mathrm{r}}}{\sigma_k^{\mathrm{r}}} C_{kk}^{\mathrm{r}}(x)\right] \mathrm{e}^{-|\overline{Z}_j - \overline{Z}_k|/\xi_z^{\mathrm{r}}} \equiv I_{jk}^{\mathrm{p}}(x, z) + I_{jk}^{\mathrm{r}}(x) \end{aligned} \tag{12}$$

where ξ_z^{p} and ξ_z^{r} are the cutoff lengths of the vertical correlations of the periodic and random roughness, respectively. Equation (11) can be rewritten as

$$C_{jk}(x, Z) = \int_{-\infty}^{+\infty} \int_{-\infty}^{+\infty} I_{jk}(x - x', Z - Z') O_{jk}(x', Z')\, \mathrm{d}x'\, \mathrm{d}Z' \tag{13}$$

where

$$O_{jk}(x, Z) = \delta(x - |\overline{Z}_j - \overline{Z}_k| \tan\theta_t)\delta(Z - |\overline{Z}_j - \overline{Z}_k|). \tag{14}$$

Fourier transforming equation (13), we obtain the out-of-plane power spectral density function

$$\tilde{C}_{jk}(q_x, q_z) = \tilde{I}_{jk}(q_x, q_z)\tilde{O}_{jk}(q_x, q_z) = \tfrac{1}{2}(\tilde{I}_{jk}^{\mathrm{p}}(q_x, q_z) + \tilde{I}_{jk}^{\mathrm{r}}(q_x))\, \mathrm{e}^{-\mathrm{i}q_x|\overline{Z}_j - \overline{Z}_k| \tan\theta_t}\, \mathrm{e}^{-\mathrm{i}q_z|\overline{Z}_j - \overline{Z}_k|} \tag{15}$$

where equations (12) and (14) have been used. It is straightforward to derive the corresponding formulae for the (q_y, q_z) plane.

We use the distorted-wave Born approximation (DWBA) method [8] to calculate the differential cross section $\mathrm{d}\sigma/\mathrm{d}\Omega$ of x-ray scattering for rough interfaces. To solve the wave equation for the scattering potential $V = V^{(\mathrm{A})} + V^{(\mathrm{B})}$, we assume a semi-infinite medium of uniform electron density with a flat surface for the undisturbed potential $V^{(\mathrm{A})}$ and a multilayer structure with rough interfaces for the disturbance $V^{(\mathrm{B})}$. The diffuse part of the differential cross section thus derived has a similar form to that obtained by as Holý *et al* [5], but the two formulations use different correlation functions $C(x, y, z)$. Our choice of the undisturbed

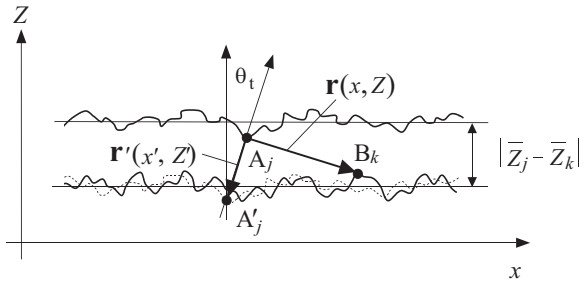

Figure 7. To derive the roughness correlation between points A_j and B_k, interface j is shifted so that the mean interface coincides with the one of interface k. The dotted curve shows the shifted interface j.

system means that we do not take into account the diffuse scattering of the reflected waves or the Bragg reflection of the diffusely scattered waves, as Holý *et al* pointed out [5].

Formula (12) means that the high-frequency fluctuations are as well correlated from one interface to the next as low-frequency fluctuations. To impart a physically more desirable property, we replace $\exp[-|\overline{Z}_j - \overline{Z}_k|/\xi_z]$ in (12) with $\exp[-|\overline{Z}_j - \overline{Z}_k|/\xi_z(1 - q_x^4/q_{xc}^4)]$, where q_{xc} is the q_x value at the critical angle for total external reflection.

4. Data analysis

To fit the collected data, we make several simplifying assumptions:

(i) the Si and $Si_{1-x}Ge_x$ layers are uniform in electron density and have equal thickness t_{SiGe} and t_{Si} respectively, throughout a superlattice;
(ii) we assume exponential distributions for $P(l)$ and $H(h)$ [11];
(iii) all $Si/Si_{1-x}Ge_x$ interfaces in a superlattice have random roughness of equal in-plane correlation cutoff lengths ξ_x^r and ξ_y^r;
(iv) both periodic and random structures in different interfaces are partially correlated with cutoff lengths ξ_z^p and ξ_z^r;
(v) the random roughness has a fractal dimension 2.5, corresponding to $h_H = 0.5$ (Hurst parameter);
(vi) at the superlattice–substrate interface, the Si(111) surface has a bunched-step structure of a 300 nm period in the in-plane direction.

$h_H = 0.5$ is likely to be too small for MBE-grown films, but the h_H value does not critically affect the fit results. Assumption (vi) is based on [10], which refers to the structure of clean vicinal Si(111) surfaces. To reduce the surface energy at room temperature, atomic steps on the 1×1 surface are bunched together to form giant steps, separated by relatively flat 7×7 reconstructed terraces. The bunch size, i.e. the number of single-height steps included in a bunch, is an insensitive function of the small miscut angle α and is reported to be about 10 [10]. This leads to the 300 nm bunch spacing for $\alpha = 0.6^\circ$.

To account for the specular reflectivity peaks in figure 2, we assume Gaussian functions of 0.35 and 0.24 mrad in half-width for samples 1 and 2 respectively, which are used to convolute the intrinsic profiles. These widths represent the combined effects of sample curvatures and the angular width of the probing x-rays. The subsidiary diffuse peaks, shown by thick arrows

in figure 3, are much broader, 2–3 mrad in half-width. To fit the peaks, we convoluted the diffuse profiles given by equation (9) with a Lorentzian function

$$\frac{1}{1+q_x^2(n_x\overline{L}_x)^2} \qquad \text{or} \qquad \frac{1}{1+q_y^2(n_y\overline{L}_y)^2} \tag{16}$$

where $n_x\overline{L}_x$ and $n_y\overline{L}_y$ represent the coherent sizes in the x and y directions respectively.

For both x and y directions, we least-squares fitted the offset-specular and rocking-scan profiles simultaneously. The results are shown by full curves in figures 2 and 3 and by grey-scale maps in the right-hand panels of figure 5, with the determined structure parameters listed in table 1. $\overline{L}_x$, σ_j^{p}, and σ_j^{r} were independent free fitting parameters for the 19 layer interfaces: our samples contain ten Si–$Si_{1-x}Ge_x$ and nine $Si_{1-x}Ge_x$–Si interfaces. $\overline{L}_x$ was fixed at 300 nm for the $Si_{1-x}Ge_x$–substrate interface. We have thus determined nineteen values for each of $\overline{L}_x$, σ_j^{p}, and σ_j^{r}. Table 1 shows the value ranges for these parameters over the 19 interfaces. The mean period $\overline{L}_x$ of the step-terrace structures shows a small variation from one interface to another in a superlattice, including the bottom Si–$Si_{1-x}Ge_x$ interface immediately above the substrate surface. It is likely that the stress-driven step redistribution took place during the growth of the first $Si_{1-x}Ge_x$ layer. In sample 2, the three times greater Ge content than in sample 1 led to a drastic change in the step configuration: the densely bunched steps on the substrate Si surface are widely dispersed at the first Si–$Si_{0.7}Ge_{0.3}$ interface. We discussed in [4] the feasibility of such step redistributions in the presence of misfit stress. The change is more moderate in sample 1, where the substrate step structure is essentially copied into the superlattice. The fluctuation exponent τ_x, 64 nm for sample 1 and 260 nm for sample 2 in table 1, represents the extent to which L_x varies around $\overline{L}_x$ in a superlattice. The greater τ_x value for sample 2 is consistent with the vanishing higher-order harmonics of the diffuse peaks in figures 3 and 5, while some harmonics are seen in sample 1.

Table 1. Structure parameters for the $[\mathrm{Si}–\mathrm{Si}_{0.9}\mathrm{Ge}_{0.1}]_{10}$ (sample 1) and $[\mathrm{Si}–\mathrm{Si}_{0.7}\mathrm{Ge}_{0.3}]_{10}$ (sample 2) superlattices determined from the x-ray diffuse scattering data. For the symbols, see text. The figures in parentheses show the standard deviations in the unit of the least-significant digit given.

Parameter	Sample 1	Sample 2
t_{Si} (nm)	4.54 (0.01)	4.20 (0.01)
t_{SiGe} (nm)	4.20 (0.01)	4.20 (0.01)
$\overline{L}_x$ (nm)	375 (1)–385 (1)	1080 (1)–1110 (6)
τ_x (nm)	64 (7)	260 (40)
$\overline{L}_y$ (nm)	898 (40)	>2000
τ_y (nm)	247 (40)	540 (60)
n_x	1.71	0.80
n_y	0.88	—
$\sigma_{\mathrm{sub}}^{\mathrm{p}}$ (nm)	0.30 (5)	0.43 (1)
σ_j^{p} (nm)	0.77 (8)–1.23 (9)	0.69 (3)–1.26 (11)
ξ_z^{p} (nm)	195 (41)	200 (8)
$\sigma_{\mathrm{sub}}^{\mathrm{r}}$ (nm)	0.20 (6)	0.09 (1)
σ_j^{r} (nm)	0.18 (1)–0.28 (5)	0.16 (3)–0.28 (7)
ξ_x^{r} (nm)	21 (2)	50 (8)
ξ_y^{r} (nm)	23 (1)	78 (14)
ξ_z^{r} (nm)	38 (8)	98 (8)
θ_{t} (°)	45 (20)	0 (2)

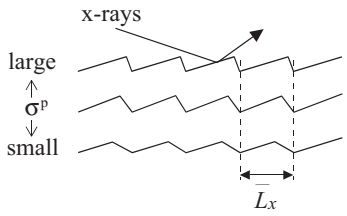

Figure 8. Scheme showing a more extended terrace area for a greater σ^{p} for a fixed $\overline{L}_x$.

In contrast to $\overline{L}_x$, the values obtained for σ_j^{p} and σ_j^{r} show fluctuations greater than 50% from one interface to another in table 1. This is due to the rougher $Si_{1-x}Ge_x$–Si interfaces than the Si–$Si_{1-x}Ge_x$ interfaces[1] for given ξ_x^{r} and ξ_y^{r}. It is surprising that $\overline{L}_x$ is only slightly different in the two types of interface.

Table 1 shows coherent lengths $n_x\overline{L}_x \approx 650$ nm and $n_y\overline{L}_y \approx 800$ nm for sample 1 and $n_x\overline{L}_x \approx 880$ nm for sample 2. It is likely that the stepped interfaces are divided into domains of these sizes along the x and y directions. The step positions in two different domains are randomly out of phase. A further discussion will be given on this point in the next section.

In [4] we discussed the asymmetric diffuse-peak heights in the q_x scans in terms of the distinct areas of the up-hill and down-hill faces of the wavy interfaces seen by incoming x-rays [13]. The σ_j^{p} values in table 1 allow us to estimate the relative face areas. With the terraces making angle α to the mean interface plane, a greater σ^{p} means more extended terraces for a given $\overline{L}_x$ in the scattering configuration shown in figure 8, which is the one used in our experiment. In sample 1 the terraces have a three times larger width than the step areas, whereas the terrace width is 35–70% of that of the step areas in sample 2. The former value is consistent with the AFM measurement that gives 2.6. The value 35–70% does not contradict the nearly equal intensities of the diffuse peaks in the $+q_x$ and $-q_x$ regions observed in sample 2 (figure 3(b)).

The ξ_z^{p} values, 195 nm and 200 nm for samples 1 and 2 respectively, are greater than the total superlattice thickness, indicating that the step-terrace structures are highly correlated in different interfaces in the two samples. The random roughness is much less correlated than the periodic structure: the ξ_z^{r} values are less than one-half of ξ_z^{p} in samples 1 and 2. The root mean square σ_j^{r} values of the random roughness are significantly smaller than σ_j^{p}, which is consistent with the AFM observation (figure 4). As to the in-plane structure, the obtained ξ_x^{r} values are smaller than the mean terrace widths in samples 1 and 2. The slightly smaller ξ_x^{r} values than the ξ_y^{r} values may indicate that the bunched steps interrupted the continuation of the random structure. Our data analysis assumed a same out-of-plane correlation direction for the periodic and random roughnesses. Table 1 shows that this direction makes a 45° angle to the surface normal in sample 1, while it is parallel in sample 2.

5. Discussion

The formulae developed in this paper are useful in exploring the structure properties of stepped interfaces in a multilayer using the x-ray diffuse scattering technique. Our formulae allow the periodic and random roughnesses to be separately evaluated, which is not feasible with Holý *et al*'s formulae [5]. We decomposed the interface roughness into the periodic and random components to derive the power spectral density functions for interfaces associated with bunched steps. We used a fractal model for the random component and the statistical distribution

[1] Here notation A/B means that the layer in the left-hand position is closer to the multilayer surface than the layer in the right-hand position.

function given by Pukite *et al* [11] for the periodic component. This is in contrast to Holý *et al* [5] who made no such decomposition but modelled the morphology of stepped interfaces by terraces and steps with statistically distributed widths l and heights h. For samples including bunched steps, the positions of subsidiary diffuse peaks in reciprocal space in the miscut direction are dictated by $\overline{L}_x$, but not by the mean terrace width ($\bar{l}$), as is the case with Holý *et al*'s formulation [5]. In the samples we investigated, $\bar{l}$ is ∼30 nm, whereas $\overline{L}_x$ is 380–1100 nm.

The calculated diffuse intensities fit generally well the experimental profiles in figure 3, but the fit is poor around the Yoneda peaks in a few profiles. This appears to arise from the excessive suppression of the scattering from the high-frequency fluctuations by the term $\exp[-|\overline{Z}_j - \overline{Z}_k|/\xi_z(1 - q_x^4/q_{xc}^4)]$ introduced in the correlation function $I_{jk}(x, z)$, which becomes zero at $q_x = q_{xc}$. The disagreement would not however significantly degrade the quality of the structure parameter determined because x-ray penetration into the sample is extremely shallow at such q_x values.

The obtained n_x values, 1.71 for sample 1 and 0.80 for sample 2, indicate that the periodic bunched step-terrace structure is of short coherence along the miscut direction, with just one or two periods included in a single domain. The $n_y = 0.88$ for sample 1 indicates that the domain size in the y direction is close to one wavelength of the step-edge meander in this sample. The two-dimensional AFM images reproduced in the previous papers [3, 4] clearly show the step meanders. The small domain size in the y direction appears to arise from the fact that the miscut direction is 10° off the $[\bar{2}11]$ direction.

In [4] we gave an extended thermodynamic discussion favouring the stress-driven redistribution of the existing steps at the vicinal substrate surface when replicated into the Si–$Si_{0.7}Ge_{0.3}$ multilayer. X-ray scattering or AFM data from the original Si surfaces before the superlattice deposition would support the discussion, but unfortunately these data are unavailable. The quite different interface structures in Si–$Si_{0.9}Ge_{0.1}$ and Si–$Si_{0.7}Ge_{0.3}$ are now evidenced by the good agreement of the calculated diffuse x-ray scattering with the observation.

Acknowledgments

We thank Y Shiraki for providing the superlattice samples. The assistance by O Sakata in the early experiments is appreciated. We appreciate the discussion with V Holý, which revealed that our expression for the scattering cross section is the same as in Holý *et al* [5] except the roughness correlation function. YY acknowledges the Hattori Foundation for the grant that supported him.

References

[1] Jesson D E, Chen K M and Pennycook S J 1996 *Mater. Res. Soc. Bull.* **21** 31–7
[2] Pidduck A R, Robbins D J, Cullis A G, Leon W Y and Pitt A M 1992 *Thin Solid Films* **222** 78
[3] Reimer P M, Li J H, Yamaguchi Y, Sakata O, Hashizume H, Usami N and Shiraki Y 1997 *J. Phys.: Condens. Matter* **9** 4521
[4] Li J H, Yamaguchi Y, Hashizume H, Usami N and Shiraki Y 1998 *J. Phys.: Condens. Matter* **10** 8643
[5] Holý V, Giannini C, Tapfer L, Marschner T and Stolz W 1997 *Phys. Rev.* B **55** 9960
[6] Barnea Z, Creagh D C, Davis T J, Garrett R F, Janky S, Stevenson A W and Wilkins S W 1992 *Rev. Sci. Instrum.* **63** 1069
[7] Holý V and Baumbach T 1994 *Phys. Rev.* B **49** 10 668
[8] Sinha S K, Sirota E B, Garoff S and Stanley H B 1988 *Phys. Rev.* B **38** 2297
[9] Phaneuf R J, Williams E D and Bartelt N C 1988 *Phys. Rev.* B **38** 1984
[10] Swartzentruber B S, Mo Y W, Webbs M B and Lagally M G 1989 *J. Vac. Sci. Technol.* A **7** 2901
[11] Pukite P R, Lent C S and Cohen P I 1985 *Surf. Sci.* **161** 39
[12] Schromka J P, Tolan M, Schwalowsky L, Seeck O H, Stettner J and Press W 1995 *Phys. Rev.* B **51** 2311
[13] Phang Y H, Teichert C, Lagally M G, Peticolos L J, Bean J C and Kasper E 1994 *Phys. Rev.* B **50** 14 435